A Steady State Continuous Flow Chamber
for the Study of Daytime and Nighttime Chemistry
under Atmospherically Relevant NO levels

Xuan Zhang [1*], John Ortega [1*], Yuanlong Huang [2], Stephen Shertz [1],
Geoffrey S. Tyndall [1], and John J. Orlando [1]

[1] Atmospheric Chemistry Observation & Modeling Laboratory (ACOM), National Center for Atmospheric Research (NCAR), Boulder, CO, USA

[2] Department of Environmental Science and Engineering, California Institute of Technology, Pasadena, CA, USA

[*] Authors contributed equally to this work.

Correspondence to: Xuan Zhang (xuanz@ucar.edu)

1 **Abstract**

2   Experiments performed in laboratory chambers have contributed significantly to the
3 understanding of the fundamental kinetics and mechanisms of the chemical reactions occurring
4 in the atmosphere. Two chemical regimes, classified as 'high-NO' versus 'zero-NO' conditions,
5 have been extensively studied in previous chamber experiments. Results derived from these two
6 chemical scenarios are widely parameterized in chemical transport models to represent key
7 atmospheric processes in urban and pristine environments. As the anthropogenic NO_x emissions
8 in the United States have decreased remarkably in the past few decades, the classic 'high-NO'
9 and 'zero-NO' conditions are no longer applicable to many regions that are constantly impacted
10 by both polluted and background air masses. We present here the development and
11 characterization of the NCAR Atmospheric Simulation Chamber, which is operated in steady
12 state continuous flow mode for the study of atmospheric chemistry under 'intermediate NO'
13 conditions. This particular chemical regime is characterized by constant sub-ppb levels of NO
14 and can be created in the chamber by precise control of the inflow NO concentration and the
15 ratio of chamber mixing to residence timescales. Over the range of conditions achievable in the
16 chamber, the lifetime of peroxy radicals (RO_2), a key intermediate from the atmospheric
17 degradation of volatile organic compounds (VOCs), can be extended to several minutes, and a
18 diverse array of reaction pathways, including unimolecular pathways and bimolecular reactions
19 with NO and HO_2, can thus be explored. Characterization experiments under photolytic and dark
20 conditions were performed and, in conjunction with model predictions, provide a basis for
21 interpretation of prevailing atmospheric processes in environments with intertwined biogenic and
22 anthropogenic activities. We demonstrate the proof of concept of the steady state continuous
23 flow chamber operation through measurements of major first-generation products, methacrolein
24 (MACR) and methyl vinyl ketone (MVK), from OH- and NO_3-initiated oxidation of isoprene.

1. Introduction

With the discovery of the role of biogenic volatile organic compounds (BVOCs) in urban photochemical smog (Chameides et al., 1988), the interactions of biogenic emissions with man-made pollution and their subsequent impact on the atmosphere's oxidative capacity and aerosol burden have received extensive studies in the ensuing decades (De Gouw et al., 2005; Ng et al., 2007; Goldstein et al., 2009; Surratt et al., 2010; Rollins et al., 2012; Shilling et al., 2013; Xu et al., 2015). A particular research focus has been understanding the influence of nitrogen oxides ($NO_x = NO + NO_2$) on the atmospheric oxidation cascades of BVOCs, which ultimately generate ozone (O_3) and secondary organic aerosols (SOA). Nitrogen oxides alter the distribution of BVOC oxidation products by primarily modulating the fate of peroxy radicals (RO_2), a key intermediate produced from the atmospheric degradation of VOCs by major oxidants including OH, O_3, and NO_3. In the absence of NO_x, RO_2 reacts predominantly with HO_2 radicals yielding organic peroxides and other products, and to a lesser extent, undergoes self/cross-reactions yielding carbonyls, alcohols, and multifunctional species. In the presence of elevated NO_x, the dominant fate of RO_2 is to react with NO leading to ozone production, and also to organic nitrates. During the night, RO_2 also reacts with NO_3 which is produced by the reaction between O_3 and NO_2. In addition, reaction of peroxyacyl radicals ($RC(O)O_2$) with NO_2 produces peroxyacyl nitrates that constitute a large reservoir of reactive nitrogen and a potentially important SOA precursor (Singh and Hanst, 1981; Nguyen et al., 2015).

Much of our understanding of the extent to which NO_x mediates the oxidation chemistry of BVOC in the atmosphere has been derived from measurements in laboratory chambers, where two extreme experimental conditions, i.e., 'high-NO' vs. 'zero-NO', were mostly performed to examine the reaction pathways of RO_2 radicals (Kroll and Seinfeld, 2008; Orlando and Tyndall, 2012; Ziemann and Atkinson, 2012). Results from these two chemical regimes have been widely incorporated into chemical transport models to represent key atmospheric processes in urban and pristine environments, respectively (Kanakidou et al., 2005). In the actual atmosphere, however, the fate of RO_2 radicals is rather more complicated than simply undergoing bimolecular reactions with NO/HO_2 as observed under the two extreme chamber conditions. It has been recently revealed that RO_2 radicals may undergo an internal H-shift followed by sequential O_2 addition, leading to highly oxygenated multifunctional peroxides (Ehn et al., 2014; Jokinen et al., 2015; Kurtén et al., 2015; Kirkby et al., 2016; Zhang et al., 2017). The rate of H-shift largely depends on the thermochemistry of the nascent alkyl radicals and can be reasonably fast, on a time scale of seconds to minutes (Crounse et al., 2013). Further, depending on the stability of the RO_2 precursor (alkyl radicals), RO_2 radicals may lose O_2 in competition with bimolecular reactions with NO, NO_3, RO_2, and HO_2. Recent theoretical and laboratory studies have found that the hydroxy peroxy radical conformers produced from isoprene photooxidation decompose readily to allylic radicals on time scales faster than bimolecular processes under atmospherically relevant NO/HO_2 levels (tens to hundreds of parts per trillion by volume). This highly dynamic system leads to formation of distinctly different products that depend on the concentrations of bimolecular reaction partners from those observed in chamber experiments under 'high-NO' and 'zero-NO' conditions (Teng et al., 2017).

Anthropogenic NO_x emissions in the United States have decreased remarkably in the past few decades (EPA, 2014), resulting in significant changes in the degradation mechanisms of BVOCs, especially in regions impacted by both background and polluted air masses such as the Southeastern United States. However, the ultimate fate of peroxy radicals in environments with

70 sub-ppb NO levels is still poorly constrained, in part due to a lack of consistent measurements
71 under well controlled conditions. Experimental approaches targeting at a controlled NO level
72 (sub-ppb to ppb) have been introduced over the years. For outdoor chambers, experiments were
73 typically performed by exposing a gas mixture of O_3/NO_x/VOCs or $HONO/NO_x$/VOCs to natural
74 sunlight (Bloss et al., 2005; Karl et al., 2006). OH radicals were produced either via the
75 photolysis of ozone and subsequent reaction of $O(^1D)$ with H_2O or directly from the photolysis
76 of HONO. NO levels ranging from a few hundreds of ppt to a few ppb over the course of several
77 hours of reactions have been reported. In the absence of any additional supply, NO will be
78 eventually depleted in a closed chamber environment, and the initial 'moderate-NO' condition
79 will essentially transfer to the 'zero-NO' condition. For indoor chambers, a 'slow chemistry'
80 scenario initiated by photolyzing methyl nitrite (CH_3ONO) under extremely low UV intensities
81 as the OH radical source ($J_{CH3ONO} \sim 10^{-5}$ s^{-1}) was created to study the autoxidation chemistry of
82 peroxy radicals produced from isoprene photooxidation (Crounse et al., 2011; Crounse et al.,
83 2012; Teng et al., 2017). The resulting NO and HO_2 mixing ratios are maintained at ~ppt level
84 ($CH_3ONO + O_2 + hv \rightarrow HO_2 + NO + HCHO$) over the course of several hours of reaction, and
85 the average OH concentration (OH ~ 10^5 molec cm^{-3}) is approximately one order of magnitude
86 lower than that in the typical daytime ambient atmosphere. Another example relates to a recent
87 method development in the Potential Aerosol Mass (PAM) flow tube reactor where nitrous oxide
88 (N_2O) was used to produce ~ppb level of NO ($O_3 + hv \rightarrow O_2 + O(^1D)$; $O(^1D) + N_2O \rightarrow 2NO$)
89 (Lambe et al., 2017). Timescales for chemical reactions and gas-particle partitioning are
90 ultimately limited to the mean residence time (~80 s) of the PAM reactor.

91   An alternative experimental platform to the batch-mode chamber and flow tube reactor
92 described above is a well-mixed steady-state chamber with continuous feed of reactants and
93 continuous withdrawal of reactor contents (Shilling et al., 2008). An attribute of the continuous
94 flow steady state chamber is that, by control of the inlet reactant concentrations and the ratio of
95 mixing to residence timescales, it is possible to simulate atmospheric oxidation under stable
96 conditions over a wide range of time periods and chemical scenarios. For example, a steady-state
97 NO level at ~1 ppb was created by the continuously mixed flow chamber operation for the study
98 of isoprene photooxidation chemistry (Liu et al., 2013). In this study, we present the
99 development and characterization of the NCAR Atmospheric Simulation Chamber, which is
100 operated in steady state continuous flow mode for simulating atmospheric daytime and nighttime
101 chemistry over chemical regimes not accessible in static chamber experiments. We focus on
102 establishing an 'intermediate NO' regime characterized by a constant steady-state NO level
103 ranging from tens of ppt to a few ppb in the chamber. This particular chemical regime is well
104 suited for the study of atmospheric behavior of RO_2 radicals, as they can survive up to minutes
105 and embrace various reaction possibilities as opposed to reaction with NO, NO_3, HO_2, and RO_2
106 as their dominant fate observed in most batch-mode chamber experiments. We employ the
107 'intermediate NO' regimes to reexamine the daytime and nocturnal chemistry of isoprene
108 through the measurements of two first-generation products, methacrolein (MACR) and methyl
109 vinyl ketone (MVK).

110 **2. Experimental**

111   **2.1 NCAR Atmospheric Simulation Chamber Facilities**

112   The NCAR Atmospheric Simulation Chamber consists of a 10 m^3 FEP Teflon (0.005" thick)
113 bag that is housed in a cubic enclosure with UV reflective surfaces and a bank of 128 wall-

114   mounted blacklight tubes (32W, Type F32T8/BL). To characterize photolytic conditions in the
115   chamber, irradiance spectra were collected in the wavelength range of 180–600 nm at ~0.8 nm
116   resolution by a custom-built spectroradiometer, as shown in Figure S1 in the Supplement
117   (Petropavlovskikh et al., 2007). Photolysis frequencies were calculated based on the measured
118   downwelling spectral actinic fluxes. The computed photolysis rate of NO_2 ($J_{NO_2} \sim 1.27 \times 10^{-3}$ s^{-1})
119   agrees within 3% with that measured by photolyzing 18.6 ppb NO_2 in the chamber and
120   monitoring the NO production rate. The chamber is equipped with a standard set of
121   measurements, including an integrated temperature and humidity probe (Model 50U, VAISALA,
122   CO) and a Magnehelic differential pressure indicating transmitter (Model 605-11, Dwyer
123   Instruments, IN). The chamber temperature is controlled at 295 K by the building's air
124   conditioning system and increases to 305–306 K under maximum irradiation conditions. The
125   relative humidity of the chamber air is below 10% under dry conditions (the remaining water
126   vapor is generated from methane combustion during the air purification process) and can be
127   varied in the range of ~10–50% by flowing a portion of the purified dry flushing air into the
128   chamber through a temperature-controlled water reservoir. Typical temperature and relative
129   humidity profiles across the chamber under maximum irradiation conditions are given in Figure
130   S1 in the Supplement. The chamber internal pressure is maintained slightly above the ambient
131   pressure to minimize the enclosure air contamination via penetration through the Teflon film.

132   Prior to each experiment, the chamber was flushed with purified dry air from an ultra high
133   purity zero air generator (Model 737, Aadco Instruments, OH) for >12 h until ozone and NO_x
134   levels were below 1 ppb. During the operation of the steady state continuous flow mode, the
135   chamber was constantly flushed with purified dry air at 40 L min^{-1}, which gives an average
136   chamber residence time of 4.17 hours. The incoming and outgoing flows were balanced by a
137   feedback control system that maintains a constant internal pressure of 1.2–4.9$\times 10^{-4}$ atm above
138   the ambient. The chamber is actively mixed by the turbulence created by the 40 L min^{-1} flushing
139   air. The characteristic mixing time is defined as the time it takes for the measurement signal of a
140   tracer compound (e.g., CO_2 and NO) to stabilize following a pulse injection. The average mixing
141   time in the NCAR chamber was determined to be ~9 min, which is ~4% of the residence time.
142   Under such conditions, the gas/particle-phase composition in the outflow can be assumed
143   identical to that in the well-mixed core of the chamber.

144   To mimic daytime photochemistry in the continuous flow mode, steady-state OH mixing
145   ratio was created by photolyzing hydrogen peroxide (H_2O_2) vapor that was continuously flowing
146   into the chamber ($H_2O_2 + h\nu \rightarrow 2OH$, $J_{H_2O_2} \sim 3.93 \times 10^{-7}$ s^{-1}). Specifically, a 20 mL syringe
147   (NORM-JECT, Henke-Sass Wolf, MA) held on a syringe pump (Model 100, kdScientific, MA)
148   kept at ~4 °C was used to deliver H_2O_2 solution (1–30 wt%, Sigma Aldrich, MO) into a glass
149   bulb that was gently warmed at ~32 °C. The liquid delivery rate was sufficiently slow (100–300
150   μL min^{-1}) that all the H_2O_2 vapor was released into the glass bulb through evaporation of a small
151   droplet hanging on the needle tip. An air stream (5 L/min) swept the H_2O_2 vapor into the
152   chamber, resulting in an H_2O_2 mixing ratio in the range of 600 ppb to 16.22 ppm in the injection
153   flow as a function of the concentration of H_2O_2 aqueous solution used. A spreadsheet (Table S2)
154   for calculating the inflow H_2O_2 mixing ratio using the above input method is provided in the
155   Supplement. As H_2O_2-laden air was continuously entering the chamber, it took approximately
156   three turnover times (~12.5 hr) for the desired H_2O_2 vapor mixing ratio to reach steady state in
157   the chamber. The H_2O_2 vapor concentration in the chamber, though not measured, can be
158   estimated from the steady-state OH mixing ratio derived from the observed exponential decay of

159 a given parent hydrocarbon. Constant NO injection flow was achieved by diluting the gas flow
160 from a concentrated NO cylinder (NO = 133.16 ppm, balance N_2) to a desired mixing ratio
161 (0.1−100 ppb) using a set of mass flow controllers (Tylan FC260 and FC262, Mykrolis Corp.,
162 MA). The lowest steady-state NO level that can be achieved in the chamber is around 30 ppt
163 (unpublished, NCAR). Note that for experiments performed in the absence of any VOC
164 precursor, H_2O_2 and NO were the only two species that were continuously input into the chamber
165 for the establishment of a combination of different photochemical conditions as denoted by the
166 O_3 and NO_x measurements. For the isoprene photooxidation experiments, an isoprene standard
167 (C_5H_8 = 531 ppm, balance N_2) was constantly injected into the chamber and diluted with the
168 flushing air to achieve an inflow concentration of ~20 ppb.

169   To mimic the nighttime chemistry in the continuous flow mode, steady-state NO_3 mixing
170 ratio was created by constantly flowing diluted O_3 and NO air into the chamber ($NO+O_3$
171 $\rightarrow NO_2+O_2$; $NO_2+O_3 \rightarrow NO_3+O_2$). The NO source can be replaced by NO_2, although the absolute
172 absence of NO does not necessarily represent the actual atmospheric conditions. O_3 was
173 produced by photolyzing O_2 in air at 185 nm using a mercury "Pen-Ray" lamp (UVP LLC, CA).
174 Ozone concentration in the injection flow can be controlled from 3.5 ppb to 457 ppb
175 automatically by adjusting the mercury lamp duty cycle. To study the RO_2+HO_2 pathway,
176 formaldehyde (CH_2O) was input into the chamber along with NO and O_3 to initiate HO_2
177 production ($NO_3+CH_2O+O_2 \rightarrow HNO_3+HO_2+CO$). Formaldehyde aqueous solution (37 wt%,
178 Sigma Aldrich, MO) was diluted with ultrapure water (Milli-Q, Merck Millipore, MA) to 0.2–1.0
179 wt% and continuously input into the chamber using the same method used for H_2O_2 input
180 described above. It is worth noting that the formaldehyde aqueous solution contains 10–15%
181 methanol as stabilizer to prevent polymerization. The presence of methanol in the chamber does
182 not significantly impact the nocturnal chemistry as it consumes OH and NO_3 radicals to generate
183 formaldehyde   and   additional HO_2 ($CH_3OH+NO_3 \rightarrow HNO_3+CH_2O+HO_2$,
184 $CH_3OH+OH \rightarrow H_2O+CH_2O+HO_2$) (Atkinson et al., 2006). The use of formaldehyde as an HO_2
185 source mimics closely the atmospheric nighttime conditions in forest environments (Schwantes
186 et al., 2015). To study the NO_3-initiated oxidation of isoprene, an injection flow of diluted
187 isoprene (~10 ppb) was achieved using the procedure described above.

2.2 Analytical measurements

189   A suite of instruments was used to monitor gas-phase concentrations in the chamber
190 outflow. O_3 was monitored by absorption spectroscopy with 0.5 ppb detection limit (Model 49,
191 Thermo Scientific, CO). The O_3 monitor was calibrated using an Ozone Primary Standard in the
192 range of 0 to 200 ppb (Model 49i-PS, Thermo Scientific, CO). The O_3 monitor used for chamber
193 experiments was periodically checked with the primary standard and was shown to be stable over
194 long periods of time (less than 1 ppb drift in over 1 year). NO was monitored by
195 chemiluminescence with 0.5 ppb detection limit (Model CLD 88Y, Eco Physics, MI). Zero-point
196 and span calibrations of the NO_x monitor were performed prior to each experiment by supplying
197 the instrument with pure N_2 gas and diluted NO, respectively. Multi-point calibration was
198 performed on a weekly basis and has shown a good stability and linearity in the NO
199 measurement ranging from 1 ppb to 200 ppb. NO_x ($NO+NO_2$) measurements were performed
200 using a photolytic converter that selectively converts NO_2 to NO upstream of the photo-
201 multiplier tube in the CLD 88Y NO monitor. This converter uses two opposing arrays of UV
202 LEDs shining into a cylindrical quartz mixing tube to achieve approximately 50% conversion of
203 NO_2 to NO per second. The total efficiency for the equipment described here is approximately

204 70% as determined by measuring calibrated NO_2 standards. The sample path always includes
205 the photolytic converter, and typical experiments cycle the power for the LED lights to switch
206 between measuring NO (lights off) and NO_x (lights on). NO_2 concentrations were then
207 determined by subtracting the NO from the adjacent NO_x measurements.

208 A customized Proton Transfer Reaction Quadrupole Mass Spectrometer (PTR-Q-MS) was
209 used to measure volatile organic compounds including isoprene (C_5H_8), methacrolein (MACR,
210 C_4H_6O), and methyl vinyl ketone (MVK, C_4H_6O). The instrument was operated at 2.3 mbar drift
211 pressure and 560 V drift voltage. Measurements reported here were obtained at a sampling rate
212 of 10 Hz. In positive-mode operation, a given analyte [M] undergoes proton transfer reaction,
213 producing an ion of the form $[M+H]^+$, that is, isoprene is detected as ion $C_5H_9^+$ (*m/z* 69) and
214 MACR and MVK are both detected as ion $C_4H_7O^+$ (*m/z* 71). The instrument background was
215 collected by sampling the chamber air for at least 30 min prior to each experiment. Measured ion
216 intensities for isoprene ($C_5H_9^+$, *m/z* 69) and MACR and MVK ($C_4H_7O^+$, *m/z* 71) were calculated
217 as the signal of each ion (counts per seconds) normalized to the total ion signal of H_3O^+. The
218 instrument sensitivities towards isoprene, MACR and MVK were calibrated with a mixture of
219 diluted gas standards. The instrument sensitivity towards MACR is identical to that of MVK, and
220 as a result, the sum of MACR and MVK concentration in the sampling air can be calculated by
221 applying one calibration factor to the measured $C_4H_7O^+$ (*m/z* 71) signal intensity. Since artifacts
222 in the measured $C_4H_7O^+$ signal can be produced through thermal decomposition of isoprene
223 oxidation products, such as the peroxides, nitrates, and epoxides, on contact with hot metal

224 surface (Liu et al., 2013; Nguyen et al., 2014b; Rivera-Rios et al., 2014), a cold-trap system was
225 used to avoid bias in the interpretation of the PTR-MS data. Specifically, a 1 m section of Teflon
226 tubing was submerged in a low temperature ethanol bath (-40 ± 2 °C) that could trap oxidized
227 products less volatile than the authentic MACR and MVK standards after steady state was
228 established in the chamber. The quantification of the sum of MACR and MVK was then based
229 on the PTR-MS measured $C_4H_7O^+$ (*m/z* 71) signal downstream of the cold-trap.

230 **3. Kinetic Modeling**

231 Reaction kinetics and mechanisms for the gas-phase photochemistry were extracted from the
232 Master Chemical Mechanism (MCMv3.3.1, accessible at http://mcm.leeds.ac.uk/MCM/). The
233 inorganic reaction scheme includes 21 species and 48 reactions; and the isoprene oxidation
234 system includes 611 species and 1974 reactions. The kinetic schemes were implemented in
235 Matlab (Mathworks) to simulate the temporal profile of a given compound *i* in the chamber
236 operated in the steady state continuous flow mode:

237
$$\frac{dC_i}{dt} \cdot \tau = C_{i,0} + P_i - C_i - \sum k_i \cdot \tau \cdot C_i \tag{Eq1}$$

238 where C_i (molec cm^{-3}) is the gas-phase concentration of compound *i* in the well-mixed core of
239 the chamber; $C_{i,0}$ (molec cm^{-3}) is the initial gas-phase concentration of compound *i* in the
240 injection flow; k_i (s^{-1}) is the pseudo-1st-order rate coefficient for a chemical reaction that
241 consumes compound *i*; τ (s) is the chamber mean residence time and can be calculated as the
242 total chamber volume divided by the incoming/outgoing flow rate; and P_i (molec cm^{-3}) is the
243 increment in the concentration of compound *i* through chemical production during one residence
244 time. Note that two terms are neglected in Equation (1), i.e., organic vapor condensation onto
245 particles and deposition on the chamber wall. This is a reasonable simplification here owing to

246   the relatively high volatility ($\geq 10^{-1}$ atm) of compounds studied (Zhang et al., 2015b; Krechmer
247   et al., 2016; Huang et al., 2018). Incorporation of these two terms into Equation (1) is feasible
248   given the vapor pressure of compound *i*, suspended particle size distribution, gas-particle and
249   gas-wall partitioning coefficient, accommodation coefficients of compound *i* on particles and
250   walls, and the effective absorbing organic masses on the wall (Zhang et al., 2014a; Zhang et al.,
251   2015b; Huang et al., 2016; McVay et al., 2016; Nah et al., 2016).

252   Model simulations used for comparison with chamber measurements were initialized using
253   experimental conditions summarized in Table S1 in the Supplement. Model input parameters for
254   all simulations include temperature (295 at dark and 306 K under irradiation), local pressure
255   (8.6×10^4 Pa), relative humidity (8% at dark and 5% under irradiation), light intensity
256   ($J_{NO_2} = 1.27 \times 10^{-3}$ s^{-1} under irradiation and 0 at dark), chamber mean residence time (4.17 h), and
257   input mixing ratios of H_2O_2 (0.11−16.2 ppm for photolytic experiments), NO (0.1−100 ppb for
258   photolytic experiments and 10−20 ppb for dark experiments), O_3 (22−225 ppb for dark
259   experiments), HCHO (0−600 ppb for dark experiments), and isoprene (19.9 ppb for photolytic
260   experiments and 10.2 ppb for dark experiments). The model was propagated numerically for 25 h
261   duration for each experiment.

4. Results and Discussions

4.1 Optimal operating conditions for daytime photochemistry

264   Figure 1 shows the model predicted steady-state mixing ratios of OH, HO_2, NO_3, NO, NO_2,
265   and O_3 in the chamber after 20 hours of photochemical reactions as a function of the H_2O_2 and
266   NO concentrations in the continuous injection flow. Six blank chamber experiments were
267   compared with simulations. In general, the model captures the evolution patterns of NO_x and O_3
268   well. The predicted mixing ratios of NO, NO_2, and O_3 agree within 69%, 11%, and 33%,
269   respectively, with the measurements (see Table S1 and Figure S2 in the Supplement). The
270   relatively large NO uncertainties originate from the measurements that were performed close to
271   the instrument detection limit (0.5 ppb).

272   Simulated steady-state mixing ratios of OH radicals ([OH]$_{ss}$) range from ~5×10^5 to ~4×10^6
273   molec cm^{-3}, which over ~4 hours chamber residence time would be roughly equivalent to ~1 h to
274   ~8 h of atmospheric OH exposure (1×10^6 molec cm^{-3}). As expected, [OH]$_{ss}$ increases with
275   increasing NO influxes due to the enhanced NO_x/O_3 cycling but decreases with increasing H_2O_2
276   influxes owing to the overwhelming reaction OH+$H_2O_2 \rightarrow H_2O$+HO_2. As a consequence, the
277   steady-state mixing ratios of HO_2 radicals ([HO$_2$]$_{ss}$) reach up to ~7×10^9 molec cm^{-3} when 16.2
278   ppm H_2O_2 is continuously injected into the chamber. If 110 ppb H_2O_2 is used instead, the
279   resulting [HO$_2$]$_{ss}$ levels fall close to the ambient range (~10^8 molec cm^{-3}).

280   Simulated steady-state NO mixing ratios in the chamber range from ~2 ppt to ~0.9 ppb from
281   combinations of 0.1−20 ppb NO and 0.11−16.22 ppm H_2O_2 in the injection flow. The ratio of
282   inflow NO concentration to the steady-state NO concentration in the chamber ranges from 5 to
283   93, demonstrating the importance of chemical removal in controlling the overall steady-state NO
284   levels. O_3 accumulation is an inevitable consequence under photolytic conditions and, for
285   example, the presence of 10 ppb O_3 leads to the chemical removal term ($k_{O_3+NO} \cdot [O_3] \cdot \tau$) in
286   Equation (1) that reduces the steady-state NO concentration by a factor of 60. It is worth noting
287   that under all simulated conditions in the continuous flow mode, O_3 (~1−126 ppb) coexists with

288 NO (~0.002–0.9 ppb). This particular chemical scenario, which is impossible to achieve in
289 batch-mode reactors due to prompt conversion of NO to NO_2, could then be used to mimic
290 ambient ozonolysis chemistry, for example, in forest regions that frequently encounter polluted
291 air masses from nearby urban areas. The steady-state mixing ratios of NO_2 ($[NO_2]_{ss}$) exhibit a
292 strong linear correlation with NO influxes. The use of less than 20 ppb NO in the injection flow
293 results in a few to tens of ppb $[NO_2]_{ss}$ that is higher than the range typically found in the ambient.
294 The potential 'quenching' effect of NO_2 on RO_2 radicals through reversible termolecular
295 reactions is discussed shortly.

296   In the so-called 'high-NO_x' chamber experiments, the NO_3 radical is an unavoidable side-
297 product when black lights are used as a representative of the solar radiation in mimicking the
298 daytime photochemistry in the troposphere. The photolysis of NO_3, although its primary sink in
299 the atmosphere, proceeds rather slowly ($J_{NO_3} \sim 1.8 \times 10^{-3}$ s^{-1}) under the present chamber
300 photolytic conditions, thereby leading to a significant accumulation of NO_3 radicals
301 (7.9×10^4–2.8×10^8 molec cm^{-3}) at steady state. The simulated NO_3/OH ratio dictates the extent to
302 which the NO_3 (nighttime) chemistry competes with the OH-initiated (daytime) photochemistry.
303 For compounds that are highly reactive towards NO_3 such as isoprene, NO_3-initiated oxidation
304 accounts for up to ~60% of the overall isoprene degradation pathways at the highest NO_3/OH
305 ratio (~255) simulated. Low concentrations of NO (< 20 ppb) and H_2O_2 (< 2 ppm) in the
306 injection flow are therefore necessary to limit the interferences of NO_3-initiated chemistry.
307 Again, taking isoprene as an example, the NO_3 oxidation pathway contributes less than 0.1% of
308 the overall isoprene degradation kinetics at the lowest NO_3/OH ratio (~0.13) simulated here.

309   Also given in Figure 1 is the calculated lifetime (τ_{RO_2}) of an RO_2 radical with respect to
310 reactions with NO and HO_2 at 306 K. In most batch-mode chamber experiments, τ_{RO_2} of only
311 several seconds or less can be achieved, due to the presence of tens to hundreds of ppb levels of
312 NO and HO_2. Here τ_{RO_2} could extend to 60 s or even longer with the continuous input of low
313 mixing ratios of H_2O_2 (≤ 110 ppb) and NO (≤ 0.2 ppb). Note that the presence of tens of ppb
314 NO_2 in the chamber might impose a 'quenching' effect on the steady state RO_2 level through
315 rapid reversible reactions ($RO_2 + NO_2 + M \leftrightarrow RO_2NO_2 + M$). We evaluate this potential 'quenching
316 effect' using ethylperoxy radical ($C_2H_5O_2$) generated from OH-oxidation of ethane as an
317 example. Simulations shown in Figure S3 in the Supplement reveal that incorporation of the
318 $C_2H_5O_2 + NO_2 + M \leftrightarrow C_2H_5O_2NO_2 + M$ reaction into the mechanism in the presence of ~1–80 ppb
319 NO_2 does not notably change the behavior of $C_2H_5O_2$ radical. One exception is the peroxyacyl
320 radical, which combines with NO_2 yielding peroxyacyl nitrate. For example, under 0.1–16 ppb
321 $[NO_2]_{ss}$ as displayed in Figure 1, we calculate that the time needed for peroxyacetyl radical
322 ($CH_3C(O)O_2$)   to   reach   equilibrium   with   peroxyacetyl   nitrate
323 ($CH_3C(O)O_2 + NO_2 + M \leftrightarrow CH_3C(O)O_2NO_2 + M$) ranges from ~1 to ~10 s, suggesting that the
324 lifetime of peroxyacyl radicals is ultimately controlled by NO_2 instead of NO/HO_2 in the reaction
325 system, and consequently, peroxyacyl radicals are not expected to be long-lived in the current
326 chamber configuration.

327   We further compare the photochemical oxidation environment created here with the
328 'intermediate-NO' conditions achieved by other chambers that employed the experimental
329 approaches introduced earlier. In terms of the oxidizing power, all approaches are capable of
330 maintaining an atmospheric relevant OH level (~10^6 molec cm^{-3}), expect the 'slow chemistry'
331 scenario that limits the photolysis rate of the OH precursor and results in an average OH mixing

332 ratio of ~10^5 molec cm^{-3} (Crounse et al., 2012; Teng et al., 2017). At comparable OH levels, the
333 overall atmospheric OH exposure achieved in the flow tube reactor is rather limited due to the
334 short residence time (e.g., ~80 s in the PAM reactor). In terms of the NO_x level, precisely
335 controlled steady-state NO concentration can be achieved for an indefinite time period by
336 operating chambers in the continuously mixed flow mode. However, NO_2 accumulates during
337 the continuous oxidation process and the resulting NO_2/NO ratio can be as much as an order of
338 magnitude higher than that achieved in the static outdoor chambers.

339 **4.2 Application to OH-initiated oxidation of isoprene**

340 Methacrolein (MACR) and methyl vinyl ketone (MVK) are major first-generation products
341 from the OH-initiated oxidation of isoprene in the presence of NO (Wennberg et al., 2018). They
342 are produced from the decomposition of β-ISOPO alkoxy radicals that are primarily formed from
343 the reaction of β-ISOPOO peroxy radicals (β-1-OH-2-OO and β-4-OH-3-OO) with NO, see
344 mechanisms displayed in Figure 2 (A). Reactions of β-ISOPOO peroxy radicals with HO_2 and
345 RO_2 also partially yield β-ISOPO alkoxy radicals that ultimately lead to MACR and MVK,
346 although these pathways are considered to be minor in the presence of hundreds to thousands of
347 ppt NO in the atmosphere. The molar yields determined from previous studies range from
348 30–35% for MVK and 20–25% for MACR under high-NO conditions (NO > 60 ppb) (Tuazon
349 and Atkinson, 1990; Paulson and Seinfeld, 1992; Miyoshi et al., 1994; Ruppert and Becker,
350 2000; Sprengnether et al., 2002; Galloway et al., 2011; Liu et al., 2013). It has been recently
351 shown that the six hydroxyl peroxy radicals (ISOPOO) produced from the initial OH addition to
352 the double bonds of isoprene undergo rapid interconversion by removal/addition of O_2 that
353 competes with bimolecular reactions under atmospherically relevant NO levels (Peeters et al.,
354 2014; Teng et al., 2017). As a result, the distribution of ISOPOO radical isomers and their
355 subsequent reaction products varies with their lifetimes with respect to bimolecular reactions. In
356 the presence of hundreds of ppb NO as done by most previous experimental studies, the reaction
357 of ISOPOO radicals with NO dominates over their interconversion, and the production of β-
358 ISOPOO peroxy radical is less favored, leading the experiments to underestimate the MACR and
359 MVK yields typically obtained in ambient conditions. Measurements by Karl et al. (2006) and
360 Liu et al. (2013) conducted at NO concentrations comparable to the moderately polluted urban
361 environment (~ 0.2 ppb in Karl et al. and ~1 ppb in Liu et al.) found higher MACR (~27% in
362 Karl et al. and ~31.8% in Liu et al.) and MVK (~41% in Karl et al. and ~44.5% in Liu et al.)
363 yields than other studies.

364 Here we perform a steady-state continuous-mode experiment to measure the production of
365 MACR and MVK from the OH-initiated oxidation of isoprene in the presence of ~0.45 ppb NO.
366 Figure 3 shows the observed and simulated temporal profiles of NO_x, O_3, C_5H_8, and C_4H_6O over
367 24 hours photooxidation of isoprene. In this experiment, C_5H_8, H_2O_2, and NO were continuously
368 fed into the chamber, with constant inflow concentrations of 19.9 ppb, 600 ppb, and 19 ppb,
369 respectively. An outgoing flow at 40 L min^{-1} continuously withdrew air from the chamber to
370 balance the pressure. After approaching steady state, the sampling tube was submerged into an
371 ethanol low temperature bath (–40±2 °C) to trap oxidized products that would otherwise undergo
372 thermal decomposition introducing interferences in the $C_4H_7O^+$ (*m/z* 71) signal. The measured
373 concentrations of C_5H_8 and C_4H_6O upon cold-trapping agree within 2.8% and 4.6% uncertainties
374 with the model simulations, see Fig.3 (C) and (D).

To calculate the total molar yield ($Y_{C_4H_6O}$) of MACR and MVK, two reactions are considered:

$$C_5H_8 + OH \xrightarrow{k_1} Y_{C_4H_6O} \cdot C_4H_6O + products \qquad (R1)$$

$$C_4H_6O + OH \xrightarrow{k_2} products \qquad (R3)$$
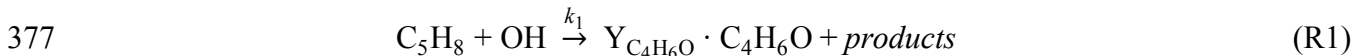
where k_1 is the rate constant for OH reaction with isoprene, and k_2 is taken as the average of rate constants for OH reactions with MACR and MVK. Uncertainties associated with the simplification of k_2 in calculating the MACR and MVK yields will be discussed shortly. Note that the ozonolysis and NO$_3$-initiated oxidation in total account for less than 6% of isoprene degradation pathway under current experimental conditions and are neglected in the calculation. The ozonolysis and photolysis in total account for ~6% of the C_4H_6O degradation pathway and are neglected here as well.

In the continuous-mode operation, two mass conservation equations are satisfied at steady state:

$$\frac{d[C_5H_8]_{ss}}{dt} = [C_5H_8]_0/\tau - [C_5H_8]_{ss}/\tau - k_1 \cdot [OH]_{ss} \cdot [C_5H_8]_{ss} = 0 \qquad (Eq2)$$

$$\frac{d[C_4H_6O]_{ss}}{dt} = Y_{C_4H_6O} \cdot k_1 \cdot [OH]_{ss} \cdot [C_5H_8]_{ss} - k_2 \cdot [OH]_{ss} \cdot [C_4H_6O]_{ss} - [C_4H_6O]_{ss}/\tau = 0 \quad (Eq3)$$

where $[C_5H_8]_{ss}$ and $[C_4H_6O]_{ss}$ are the PTRMS measured steady-state concentrations of isoprene and the sum of MACR and MVK when using the cold trap, respectively, $[C_5H_8]_0$ is the initial concentration of isoprene, and τ is the chamber mean residence time and can be calculated as the total chamber volume divided by the incoming/outgoing flow rate. The steady state OH radical concentration ($[OH]_{ss}$) can be derived by solving Equation (2). The calculated $[OH]_{ss}$ (3.13×10^6 molec cm^{-3}) is 12% higher than the model prediction (2.74×10^6 molec cm^{-3}). The molar yield of the sum of MACR and MVK from isoprene OH oxidation pathway in the presence of ~0.45 ppb NO is thus given by Equation (4) and calculated as 76.7±5.8%:

$$Y_{C_4H_6O} = \frac{[C_4H_6O]_{ss} + k_2 \cdot [OH]_{ss} \cdot \tau \cdot [C_4H_6O]_{ss}}{k_1 \cdot [OH]_{ss} \cdot \tau \cdot [C_5H_8]_{ss}} \times f_{\beta\text{-ISOPOO+NO}} \qquad (Eq4)$$

Here a 5.8% uncertainty originates from the assumption that MACR+OH and MVK+OH proceed with equal reaction rate, although the rate constant for MVK+OH is ~31% lower than that of MACR+OH. Another potential uncertainty relates to the accuracy of the simulated steady state HO$_2$ and RO$_2$ concentrations and the contribution of β-ISOPOO+HO$_2$ and β-ISOPOO+RO$_2$ reaction pathways to the overall β-ISOPOO fate. The fraction of β-ISOPOO radicals that reacts with NO ($f_{\beta\text{-ISOPOO+NO}}$) was predicted as 0.88, which was used here to scale the final MACR+MVK yield, see Eq(4).

In summary, the measured yield of the sum of MACR and MVK in this study is close to that reported by Karl et al. (2006) and Liu et al. (2013), but ~27−52% higher than the majority of previous measurements performed under high-NO conditions (NO > 60 ppb). This is consistent with the dynamic nature of the six ISOPOO radical isomers that undergo rapid interconversion by addition/removal of O$_2$. In the presence of ~0.45 ppb NO as performed in this study, lifetimes of the β-1-OH-2-OO peroxy radical with respect to reaction with NO and loss of O$_2$ are

412 estimated as 9.4 s and 0.2 s, respectively, implying that the rapid interconversion between β-
413 ISOPOO and δ-ISOPOO radicals essentially governs their distribution, and under such
414 conditions, the production of thermodynamically more stable β-ISOPOO isomers is favored,
415 leading to higher yields of MACR and MVK. Here the reported MACR and MVK yield from
416 isoprene OH oxidation in the presence of ~0.45 ppb NO represents an illustration of chamber
417 operation at steady state continuous flow mode for the establishment of certain experimental
418 conditions that are not easily accessible from traditional batch-mode chamber experiments. A
419 complete measurement of first-generation oxidation products from isoprene OH reaction under a
420 wide range of NO levels (ISOPOO bimolecular lifetimes) will be forthcoming in a future
421 publication.

422 **4.3 Optimal operating conditions for nighttime chemistry**

423   Figure 4 shows the model simulated steady-state mixing ratios of HO_2, NO_3, NO, NO_2, and
424 O_3 after 16 hours of dark reactions in the chamber as a function of the HCHO concentration and
425 O_3/NO ratio in the continuous chamber inflow. Blank experiments were compared with
426 simulations in five cases (see Table S1 in the Supplement). The model captures the evolution
427 patterns of NO_x and O_3 well. The observed mixing ratios of NO_2 and O_3 agree with the
428 simulations to within 11% and 6%, respectively (Figure S4 in the Supplement).

429   Compared with the photochemical reaction schemes discussed earlier, the nocturnal
430 chemistry is rather straightforward; that is, the inflow O_3/NO ratio governs the steady-state
431 concentrations of NO_3, NO_x, and O_3, while the inflow HCHO concentration ultimately controls
432 the steady-state HO_2 level. Increasing the O_3/NO ratio from 1 to 9 in the continuous inflow leads
433 to increased NO_3 from 2.4×10^5 to 1.1×10^9 molec cm^{-3}, but decreased NO from 1.8 ppb to 20 ppt
434 and decreased NO_2 from 18 to 7 ppb. At a fixed inflow O_3/NO ratio, doubling the NO and O_3
435 concentrations leads to elevated NO_3, NO_x, and O_3 by a factor of 2.0–3.2, 1.5–2.0, and 1.4–2.0,
436 respectively. The use of HCHO as an effective dark HO_2 source does not significantly impact the
437 steady-state mixing ratios of NO_x and O_3, but slightly weakens the NO_3 production.

438   The calculated RO_2 lifetime (τ_{RO_2}) with respect to reactions with NO, NO_3, and HO_2 at 295
439 K ranges from 3 to 225 s. The highest τ_{RO_2} was achieved in the absence of any HCHO source
440 and corresponds to a chemical regime that can be employed to study the intramolecular
441 isomerization (autoxidation) pathway of RO_2 radicals, if any. Adding a continuous flow of
442 HCHO to the system leads to the production of 10^7–10^9 molec cm^{-3} HO_2 radicals that then
443 constitute a significant sink of RO_2 radicals and represents prevailing forest environments during
444 nighttime.

445 **4.4 Application to NO_3-initiated oxidation of isoprene**

446   NO_3-initiated oxidation of isoprene proceeds by the NO_3 addition to the carbon double
447 bonds followed by O_2 addition, yielding six distinct nitrooxy peroxy radicals (INOO), including
448 two isomers (β-INOO) with O_2 added on the β-carbon to the nitrate group (see Figure 2B for
449 schematic illustration). The β-INOO radicals react further with NO_3, HO_2, NO, and RO_2,
450 producing nitrooxy alkoxy radicals (β-INO) with molar yields of 1.00, 0.53, 0.97, and 0.40,
451 respectively (Wennberg et al., 2018). The further decomposition of β-INO radicals produces
452 MACR and MVK, together with HCHO and NO_2. Depending on the actual fate of β-INOO
453 radicals, the yields of β-INO radicals can then vary from 0.4 to 1.0, resulting in a distinct
454 distribution of final oxidation products. It is thus important to specify the ultimate fate of INOO

455 radicals during quantification of oxidation products from isoprene reaction with NO_3. As an
456 illustration, we performed one continuous mode experiment that targets on controlling the
457 steady-state fate of INOO radicals to be their reaction with NO and HO_2 (46% and 38% INOO
458 radicals are predicted to react with NO and HO_2, respectively, as shown in Fig.5). Note that by
459 adjusting the concentrations and fractions of inflow reactants (O_3, NO, HCHO, and C_5H_8),
460 different chemical fates and lifetimes of INOO radicals can be achieved.

461 Figure 5 shows the observed and predicted temporal profiles of NO_x, O_3, C_5H_8, and C_4H_6O
462 over 25 hours of isoprene oxidation by NO_3, with continuous input of 10.2 ppb C_5H_8, 205 ppb
463 O_3, and 59 ppb NO into the chamber and a balancing outgoing flow at 40 L min^{-1} carrying well-
464 mixed reactants and products. It took >16 hours to reach steady state for all the species
465 displayed. In general, the model captures the trends of O_3 and NO well, while underpredicting
466 the steady state NO_2 by ~26%. After ~18 hours of dark reaction, the PTR-MS sampling tubing
467 was submerged into an ethanol cold bath (– 40±2 °C) to trap artifacts in the PTR-MS measured
468 $C_4H_7O^+$ (*m/z* 71) signal. The simulated steady-state concentration of isoprene agrees within 9%
469 with the measurements. The derived concentration of the sum of MACR and MVK from the
470 measured $C_4H_7O^+$ ion intensity upon cold-trapping is ~1.1 ppb, which is ~129% higher than the
471 model predictions (~0.48 ppb). This disagreement can be attributed, to a large extent, to the
472 oversimplified representation of the six different INOO radicals as one δ-INOO isomer in the
473 MCMv3.3.1 mechanism. As a result, the production of β-INOO radical, the important precursor
474 of MACR and MVK, from NO_3-initiated oxidation of isoprene is suppressed in the simulations.
475 The measured molar yield of the sum of MACR and MVK is 36.3±12.1%, with uncertainties
476 arising from the fact that 10.5% isoprene is predicted to react with OH as an additional source of
477 MACR and MVK. Using this value, the fraction of β-INOO over the sum of nitrooxy peroxy
478 radicals is estimated as 48.6±16.2%, which is close to that (~46.3%) reported by Schwantes et al.
479 (2015), although the estimated bimolecular lifetime of INOO radical in that study (~30 s) is
480 lower than that predicted in the present work (~50 s). As discussed above, the hydroxyl peroxy
481 radicals produced from OH-oxidation of isoprene could undergo rapid interconversion through
482 addition/removal of O_2 at atmospherically relevant lifetimes. This interconversion significantly
483 impacts the subsequent chemistry of individual ISOPOO radical isomers in terms of reaction
484 rates and product distributions. It is likely that the INOO radicals follow similar interconversion
485 due to the small R-OO bond dissociation energy, although no experimental evidence exists. A
486 full examination of the INOO chemistry, i.e., their kinetic and thermodynamic properties as well
487 as their chemical fate at different lifetimes, will be the focus of future studies using this
488 continuous flow chamber operation method.

5. Conclusions

490 We report here the development and characterization of the NCAR Atmospheric Simulation
491 Chamber operated at steady state continuous flow mode for simulating daytime and nocturnal
492 chemistry under atmospherically relevant NO levels. The chamber is designed to achieve a well-
493 controlled steady-state environment by continuous inflow of reactants and continuous
494 withdrawal of reactor contents. We use a combination of kinetic modeling and chamber
495 experiments to characterize the 'intermediate-NO' chemical regime (tens of ppt to a few ppb)
496 that can be achieved by precisely controlling the inlet reactant concentrations and the
497 mixing/residence timescales of the chamber.

498   To mimic daytime photochemistry, continuous input of H_2O_2 and NO gases is required,
499   resulting in steady state OH mixing ratios of $10^5–10^6$ molec cm^{-3} under irradiation. Under such
500   conditions, the lifetime of a peroxy radical with respect to reaction with NO and HO_2 can be
501   extended to 60 s or even longer, thus providing a unique environment to study all reaction
502   possibilities of RO_2 radicals including the intramolecular isomerization (autoxidation) pathway.
503   When studying OH-initiated chemistry, care needs to be taken to avoid a range of experimental
504   conditions (e.g., inflow $H_2O_2 > 2$ ppm and NO > 20 ppb) where NO_3-oxidation might account for
505   a large fraction of the overall degradation pathway of certain parent hydrocarbons such as
506   alkenes.

507   To mimic nighttime chemistry, continuous input of NO (or NO_2) and O_3 is needed to
508   produce steady state NO_3 radicals in the range of $10^6–10^9$ molec cm^{-3} in the dark. Under such
509   conditions, an RO_2 radical can live up to 4 min prior to finding a bimolecular reaction partner
510   (e.g., NO, NO_3, and HO_2), which were the dominant fates of RO_2 radicals in most batch-mode
511   chamber experiments. Again, the long lifetime of RO_2 radicals achieved by the steady state
512   continuous mode operation opens an avenue for close examination of RO_2 unimolecular
513   (isomerization) pathways in nocturnal environments.

514   In simulating both daytime and nighttime chemistry with continuous flow operation method,
515   O_3 accumulation is unavoidable. The extent to which ozonolysis interferes with OH- or NO_3-
516   initiated oxidation chemistry depends on the steady state O_3 concentration achieved in the
517   chamber and its reactivity towards various parent VOCs. Taking isoprene as an example,
518   ozonolysis accounts for <1% and <0.1% of the overall isoprene degradation kinetics,
519   respectively, under established steady-state photolytic and dark conditions described above.

520   In atmospheric chemistry, the terms 'zero-NO' versus 'high-NO' have been widely used to
521   classify photooxidation conditions and delineate the gas-phase fate of the peroxy radicals (RO_2)
522   generated from VOCs oxidation (Zhang et al., 2010; He et al., 2011; Cappa et al., 2013; Zhang
523   and Seinfeld, 2013; Loza et al., 2014; Nguyen et al., 2014a; Schilling Fahnestock et al., 2014;
524   Zhang et al., 2014b; Krechmer et al., 2015; Zhang et al., 2015a; Gordon et al., 2016; Riva et al.,
525   2016; Thomas et al., 2016; Schwantes et al., 2017a; Schwantes et al., 2017b). In the so-called
526   'high-NO' regime, reaction with NO dominates the fate of RO_2 radicals, whereas in the 'zero-
527   NO' regime, the RO_2 radicals primarily undergo reaction with HO_2 and, perhaps to a much lesser
528   degree, self/cross-combination. The importance of the 'intermediate-NO' regime lies in the fact
529   that at sub-ppb levels of NO, the RO_2+NO and RO_2+HO_2 reactions are expected to co-exist and
530   the RO_2 radical could survive up to several minutes before encountering a partner (NO/HO_2) for
531   bimolecular reactions. Under such conditions, the RO_2 radical isomers may undergo
532   interconversion by addition/removal of O_2 and intramolecular isomerization (autoxidation)
533   through H-shift. Here we use isoprene as an illustrative VOC to explore the fate of RO_2 radicals
534   under sub-ppb NO. Future work will focus on detailed characterization of oxidation products
535   from isoprene day- and nighttime chemistry with particular attention given to the controlled RO_2
536   fates and lifetimes.

Data Availability

538   Data presented in this manuscript are available upon request to the corresponding author.

Competing interests

The authors declare that they have no conflict of interest.

Acknowledgement

The National Center for Atmospheric Research is operated by the University Corporation for Atmospheric Research, under the sponsorship of the National Science Foundation.

Reference:

Atkinson, R., Baulch, D. L., Cox, R. A., Crowley, J. N., Hampson, R. F., Hynes, R. G., Jenkin, M. E., Rossi, M. J., Troe, J., and Subcommittee, I.: Evaluated kinetic and photochemical data for atmospheric chemistry: Volume II–gas phase reactions of organic species, Atmos. Chem. Phys., 6, 3625-4055, 2006.

Bloss, C., Wagner, V., Bonzanini, A., Jenkin, M. E., Wirtz, K., Martin-Reviejo, M., and Pilling, M. J.: Evaluation of detailed aromatic mechanisms (MCMv3 and MCMv3.1) against environmental chamber data, Atmos. Chem. Phys., 5, 623-639, 2005.

Cappa, C. D., Zhang, X., Loza, C. L., Craven, J. S., Lee, Y. D., and Seinfeld, J. H.: Application of the statistical oxidation model (SOM) to secondary organic aerosol formation from photooxidation of C12 alkanes, Atmos. Chem. Phys., 13, 1591-1606, 2013.

Chameides, W. L., Lindsay, R. W., Richardson, J., and Kiang, C. S.: The role of biogenic hydrocarbons in urban photochemical smog: Atlanta as a case study, Science, 241, 1473-1476, 1988.

Crounse, J. D., Paulot, F., Kjaergaard, H. G., and Wennberg, P. O.: Peroxy radical isomerization in the oxidation of isoprene, Phys. Chem. Chem. Phys., 13, 13607-13613, 2011.

Crounse, J. D., Knap, H. C., Ørnsø, K. B., Jørgensen, S., Paulot, F., Kjaergaard, H. G., and Wennberg, P. O.: Atmospheric fate of methacrolein. 1. Peroxy radical isomerization following addition of OH and O2, J. Phys. Chem. A, 116, 5756-5762, 2012.

Crounse, J. D., Nielsen, L. B., Jørgensen, S., Kjaergaard, H. G., and Wennberg, P. O.: Autoxidation of organic compounds in the atmosphere, J. Phys. Chem. Lett., 4, 3513-3520, 2013.

De Gouw, J. A., Middlebrook, A. M., Warneke, C., Goldan, P. D., Kuster, W. C., Roberts, J. M., Fehsenfeld, F. C., Worsnop, D. R., Canagaratna, M. R., and Pszenny, A. A. P.: Budget of organic carbon in a polluted atmosphere: Results from the New England Air Quality Study in 2002, J. Geophys. Res. Atmos., 110, 10.1029/2004JD005623, 2005.

Ehn, M., Thornton, J. A., Kleist, E., Sipilä, M., Junninen, H., Pullinen, I., Springer, M., Rubach, F., Tillmann, R., Lee, B., Lopez-Hilfiker, F., Andres, S., Acir, I.-H., Rissanen, M., Jokinen, T., Schobesberger, S., Kangasluoma, J., Kontkanen, J., Nieminen, T., Kurtén, T., Nielsen, L. B., Jørgensen, S., Kjaergaard, H. G., Canagaratna, M., Maso, M. D., Berndt, T., Petäjä, T., Wahner, A., Kerminen, V.-M., Kulmala, M., Worsnop, D. R., Wildt, J., and Mentel, T. F.: A large source of low-volatility secondary organic aerosol, Nature, 506, 476, 10.1038/nature13032, 2014.

EPA: Data from the 2011 National Emissions Inventory, Version 1. Accessed 2014. https://http://www.epa.gov/air-emissions-inventories/2011-national-emissions-inventory-nei-data., 2014.

578 Galloway, M. M., Huisman, A. J., Yee, L. D., Chan, A. W. H., Loza, C. L., Seinfeld, J. H., and
579 Keutsch, F. N.: Yields of oxidized volatile organic compounds during the OH radical initiated
580 oxidation of isoprene, methyl vinyl ketone, and methacrolein under high-NO x conditions,
581 Atmos. Chem. Phys., 11, 10779-10790, 2011.

582 Goldstein, A. H., Koven, C. D., Heald, C. L., and Fung, I. Y.: Biogenic carbon and
583 anthropogenic pollutants combine to form a cooling haze over the southeastern United States,
584 Proc. Natl. Acad. Sci. USA, 106, 8835-8840, 2009.

585 Gordon, H., Sengupta, K., Rap, A., Duplissy, J., Frege, C., Williamson, C., Heinritzi, M., Simon,
586 M., Yan, C., Almeida, J., Tröstl, J., Nieminen, T., Ortega, I. K., Wagner, R., Dunne, E. M.,
587 Adamov, A., Amorim, A., Bernhammer, A.-K., Bianchi, F., Breitenlechner, M., Brilke, S., Chen,
588 X., Craven, J. S., Dias, A., Ehrhart, S., Fischer, L., Flagan, R. C., Franchin, A., Fuchs, C., Guida,
589 R., Hakala, J., Hoyle, C. R., Jokinen, T., Junninen, H., Kangasluoma, J., Kim, J., Kirkby, J.,
590 Krapf, M., Kürten, A., Laaksonen, A., Lehtipalo, K., Makhmutov, V., Mathot, S., Molteni, U.,
591 Monks, S. A., Onnela, A., Peräkylä, O., Piel, F., Petäjä, T., Praplan, A. P., Pringle, K. J.,
592 Richards, N. A. D., Rissanen, M. P., Rondo, L., Sarnela, N., Schobesberger, S., Scott, C. E.,
593 Seinfeld, J. H., Sharma, S., Sipilä, M., Steiner, G., Stozhkov, Y., Stratmann, F., Tomé, A.,
594 Virtanen, A., Vogel, A. L., Wagner, A. C., Wagner, P. E., Weingartner, E., Wimmer, D.,
595 Winkler, P. M., Ye, P., Zhang, X., Hansel, A., Dommen, J., Donahue, N. M., Worsnop, D. R.,
596 Baltensperger, U., Kulmala, M., Curtius, J., and Carslaw, K. S.: Reduced anthropogenic aerosol
597 radiative forcing caused by biogenic new particle formation, Proc. Natl. Acad. Sci. USA, 113,
598 12053-12058, 2016.

599 He, S., Chen, Z., and Zhang, X.: Photochemical reactions of methyl and ethyl nitrate: a dual role
600 for alkyl nitrates in the nitrogen cycle, Environ. Chem., 8, 529-542, 2011.

601 Huang, D. D., Zhang, X., Dalleska, N. F., Lignell, H., Coggon, M. M., Chan, C. M., Flagan, R.
602 C., Seinfeld, J. H., and Chan, C. K.: A note on the effects of inorganic seed aerosol on the
603 oxidation state of secondary organic aerosol—α-pinene ozonolysis, J. Geophys. Res. Atmos.,
604 121, 12476-12483, 2016.

605 Huang, Y., Zhao, R., Charan, S. M., Kenseth, C. M., Zhang, X., and Seinfeld, J. H.: Unified
606 theory of vapor-wall mass transport in Teflon-walled environmental chambers, Environ. Sci.
607 Technol., 52, 2134-2142, 2018.

608 Jokinen, T., Berndt, T., Makkonen, R., Kerminen, V.-M., Junninen, H., Paasonen, P., Stratmann,
609 F., Herrmann, H., Guenther, A. B., and Worsnop, D. R.: Production of extremely low volatile
610 organic compounds from biogenic emissions: Measured yields and atmospheric implications,
611 Proc. Natl. Acad. Sci. USA, 112, 7123-7128, 2015.

612 Kanakidou, M., Seinfeld, J. H., Pandis, S. N., Barnes, I., Dentener, F. J., Facchini, M. C.,
613 Dingenen, R. V., Ervens, B., Nenes, A., and Nielsen, C. J.: Organic aerosol and global climate
614 modelling: a review, Atmos. Chem. Phys., 5, 1053-1123, 2005.

615 Karl, M., Dorn, H. P., Holland, F., Koppmann, R., Poppe, D., Rupp, L., Schaub, A., and Wahner,
616 A.: Product study of the reaction of OH radicals with isoprene in the atmosphere simulation
617 chamber SAPHIR, J. Atmos. Chem., 55, 167-187, 2006.

618 Kirkby, J., Duplissy, J., Sengupta, K., Frege, C., Gordon, H., Williamson, C., Heinritzi, M.,
619 Simon, M., Yan, C., João, A., Tröstl, J., Nieminen, T., Ortega, I. K., Wagner, R., Adamov, A.,

Amorim, A., Bernhammer, A.-K., Bianchi, F., Breitenlechner, M., Brilke, S., Chen, X., Craven, J., Dias, A., Ehrhart, S., Flagan, R. C., Franchin, A., Fuchs, C., Guida, R., Hakala, J., Hoyle, C. R., Jokinen, T., Junninen, H., Kangasluoma, J., Kim, J., Krapf, M., Kürten, A., Laaksonen, A., Lehtipalo, K., Makhmutov, V., Mathot, S., Molteni, U., Onnela, A., Peräkylä, O., Piel, F., Petäjä, T., Praplan, A. P., Pringle, K., Rap, A., Richards, N. A. D., Riipinen, I., Rissanen, M. P., Rondo, L., Sarnela, N., Schobesberger, S., Scott, C. E., Seinfeld, J. H., Sipilä, M., Steiner, G., Stozhkov, Y., Stratmann, F., Tomé, A., Virtanen, A., Vogel, A. L., Wagner, A. C., Wagner, P. E., Weingartner, E., Wimmer, D., Winkler, P. M., Ye, P., Zhang, X., Hansel, A., Dommen, J., Donahue, N. M., Worsnop, D. R., Baltensperger, U., Kulmala, M., Carslaw, K. S., and Curtius, J.: Ion-induced nucleation of pure biogenic particles, Nature, 533, 521-526, 2016.

Krechmer, J. E., Coggon, M. M., Massoli, P., Nguyen, T. B., Crounse, J. D., Hu, W., Day, D. A., Tyndall, G. S., Henze, D. K., Rivera-Rios, J. C., Nowak, J. B., Kimmel, J. R., III, R. L. M., Stark, H., Jayne, J. T., Sipila, M., Junninen, H., Clair, J. M. S., Zhang, X., Feiner, P. A., Zhang, L., Miller, D. O., Brune, W. H., Keutsch, F. N., Wennberg, P. O., Seinfeld, J. H., Worsnop, D. R., Jimenez, J. L., and Canagaratna, M. R.: Formation of low volatility organic compounds and secondary organic aerosol from isoprene hydroxyhydroperoxide low-NO oxidation, Environ. Sci. Technol., 49, 10330-10339, 2015.

Krechmer, J. E., Pagonis, D., Ziemann, P. J., and Jimenez, J. L.: Quantification of gas-wall partitioning in Teflon environmental chambers using rapid bursts of low-volatility oxidized species generated in situ, Environ. Sci. Technol., 50, 5757-5765, 2016.

Kroll, J. H., and Seinfeld, J. H.: Chemistry of secondary organic aerosol: Formation and evolution of low-volatility organics in the atmosphere, Atmos. Environ., 42, 3593-3624, 2008.

Kurtén, T., Rissanen, M. P., Mackeprang, K., Thornton, J. A., Hyttinen, N., Jørgensen, S., Ehn, M., and Kjaergaard, H. G.: Computational study of hydrogen shifts and ring-opening mechanisms in α-pinene ozonolysis products, J. Phys. Chem. A, 119, 11366-11375, 2015.

Lambe, A., Massoli, P., Zhang, X., Canagaratna, M., Nowak, J., Daube, C., Yan, C., Nie, W., Onasch, T., Jayne, J., Kolb, C., Davidovits, P., Worsnop, D., and Brune, W.: Controlled nitric oxide production via $O(1D)+N2O$ reactions for use in oxidation flow reactor studies, Atmos. Meas. Tech., 10, 2283-2298, 2017.

Liu, Y. J., Herdlinger-Blatt, I., McKinney, K. A., and Martin, S. T.: Production of methyl vinyl ketone and methacrolein via the hydroperoxyl pathway of isoprene oxidation, Atmos. Chem. Phys., 13, 5715-5730, 2013.

Loza, C. L., Craven, J. S., Yee, L. D., Coggon, M. M., Schwantes, R. H., Shiraiwa, M., Zhang, X., Schilling, K. A., Ng, N. L., and Canagaratna, M. R.: Secondary organic aerosol yields of 12-carbon alkanes, Atmos. Chem. Phys., 14, 1423-1439, 2014.

McVay, R. C., Zhang, X., Aumont, B., Valorso, R., Camredon, M., La, Y. S., Wennberg, P. O., and Seinfeld, J. H.: SOA formation from the photooxidation of α-pinene: systematic exploration of the simulation of chamber data, Atmos. Chem. Phys., 16, 2785-2802, 2016.

Miyoshi, A., Hatakeyama, S., and Washida, N.: OH radical-initiated photooxidation of isoprene: An estimate of global CO production, J. Geophys. Res. Atmos., 99, 18779-18787, 1994.

Nah, T., McVay, R. C., Zhang, X., Boyd, C. M., Seinfeld, J. H., and Ng, N. L.: Influence of seed aerosol surface area and oxidation rate on vapor wall deposition and SOA mass yields: a case study with α-pinene ozonolysis, Atmos. Chem. Phys., 16, 9361-9379, 2016.

Ng, N. L., Chhabra, P. S., Chan, A. W. H., Surratt, J. D., Kroll, J. H., Kwan, A. J., McCabe, D. C., Wennberg, P. O., Sorooshian, A., and Murphy, S. M.: Effect of NOx level on secondary organic aerosol (SOA) formation from the photooxidation of terpenes, Atmos. Chem. Phys., 7, 5159-5174, 2007.

Nguyen, T. B., Coggon, M. M., Bates, K. H., Zhang, X., Schwantes, R. H., Schilling, K. A., Loza, C. L., Flagan, R. C., Wennberg, P. O., and Seinfeld, J. H.: Organic aerosol formation from the reactive uptake of isoprene epoxydiols (IEPOX) onto non-acidified inorganic seeds, Atmos. Chem. Phys., 14, 3497-3510, 2014a.

Nguyen, T. B., Crounse, J. D., Schwantes, R. H., Teng, A. P., Bates, K. H., Zhang, X., St Clair, J. M., Brune, W. H., Tyndall, G. S., and Keutsch, F. N.: Overview of the Focused Isoprene eXperiment at the California Institute of Technology (FIXCIT): mechanistic chamber studies on the oxidation of biogenic compounds, Atmos. Chem. Phys., 14, 13531-13549, 2014b.

Nguyen, T. B., Bates, K. H., Crounse, J. D., Schwantes, R. H., Zhang, X., Kjaergaard, H. G., Surratt, J. D., Lin, P., Laskin, A., and Seinfeld, J. H.: Mechanism of the hydroxyl radical oxidation of methacryloyl peroxynitrate (MPAN) and its pathway toward secondary organic aerosol formation in the atmosphere, Phys. Chem. Chem. Phys., 17, 17914-17926, 2015.

Orlando, J. J., and Tyndall, G. S.: Laboratory studies of organic peroxy radical chemistry: an overview with emphasis on recent issues of atmospheric significance, Chem. Soc. Rev., 41, 6294-6317, 2012.

Paulson, S. E., and Seinfeld, J. H.: Development and evaluation of a photooxidation mechanism for isoprene, J. Geophys. Res. Atmos., 97, 20703-20715, 1992.

Peeters, J., Müller, J.-F. o., Stavrakou, T., and Nguyen, V. S.: Hydroxyl radical recycling in isoprene oxidation driven by hydrogen bonding and hydrogen tunneling: The upgraded LIM1 mechanism, J. Phys. Chem. A, 118, 8625-8643, 2014.

Petropavlovskikh, I., Shetter, R., Hall, S., Ullmann, K., and Bhartia, P. K.: Algorithm for the charge-coupled-device scanning actinic flux spectroradiometer ozone retrieval in support of the Aura satellite validation, J. Appl. Remote Sens, 1, 10.1117/1.2802563, 2007.

Riva, M., Budisulistiorini, S. H., Chen, Y., Zhang, Z., D'Ambro, E. L., Zhang, X., Gold, A., Turpin, B. J., Thornton, J. A., and Canagaratna, M. R.: Chemical characterization of secondary organic aerosol from oxidation of isoprene hydroxyhydroperoxides, Environ. Sci. Technol., 50, 9889-9899, 2016.

Rivera-Rios, J. C., Nguyen, T. B., Crounse, J. D., Jud, W., St Clair, J. M., Mikoviny, T., Gilman, J. B., Lerner, B. M., Kaiser, J. B., and Gouw, J. d.: Conversion of hydroperoxides to carbonyls in field and laboratory instrumentation: Observational bias in diagnosing pristine versus anthropogenically controlled atmospheric chemistry, Geophys. Res. Lett., 41, 8645-8651, 2014.

Rollins, A. W., Browne, E. C., Min, K. E., Pusede, S. E., Wooldridge, P. J., Gentner, D. R., Goldstein, A. H., Liu, S., Day, D. A., and Russell, L. M.: Evidence for NOx control over nighttime SOA formation, Science, 337, 1210-1212, 2012.

701 Ruppert, L., and Becker, K. H.: A product study of the OH radical-initiated oxidation of
702 isoprene: Formation of C 5-unsaturated diols, Atmos. Environ., 34, 1529-1542, 2000.

703 Schilling Fahnestock, K. A., Yee, L. D., Loza, C. L., Coggon, M. M., Schwantes, R., Zhang, X.,
704 Dalleska, N. F., and Seinfeld, J. H.: Secondary organic aerosol composition from C12 alkanes, J.
705 Phys. Chem. A, 119, 4281-4297, 2014.

706 Schwantes, R. H., Teng, A. P., Nguyen, T. B., Coggon, M. M., Crounse, J. D., St. Clair, J. M.,
707 Zhang, X., Schilling, K. A., Seinfeld, J. H., and Wennberg, P. O.: Isoprene NO3 oxidation
708 products from the RO2+ HO2 Pathway, J. Phys. Chem. A, 119, 10158-10171, 2015.

709 Schwantes, R. H., McVay, R. C., Zhang, X., Coggon, M. M., Lignell, H., Flagan, R. C.,
710 Wennberg, P. O., and Seinfeld, J. H.: Science of the environmental chamber, Advances in
711 Atmospheric Chemistry, 1, 1-93, 2017a.

712 Schwantes, R. H., Schilling, K. A., McVay, R. C., Lignell, H., Coggon, M. M., Zhang, X.,
713 Wennberg, P. O., and Seinfeld, J. H.: Formation of highly oxygenated low-volatility products
714 from cresol oxidation, Atmos. Chem. Phys., 17, 3453-3474, 2017b.

715 Shilling, J. E., Chen, Q., King, S. M., Rosenoern, T., Kroll, J. H., Worsnop, D. R., McKinney, K.
716 A., and Martin, S. T.: Particle mass yield in secondary organic aerosol formed by the dark
717 ozonolysis of α-pinene, Atmos. Chem. Phys., 8, 2073-2088, 2008.

718 Shilling, J. E., Zaveri, R. A., Fast, J. D., Kleinman, L., Alexander, M. L., Canagaratna, M. R.,
719 Fortner, E., Hubbe, J. M., Jayne, J. T., and Sedlacek, A.: Enhanced SOA formation from mixed
720 anthropogenic and biogenic emissions during the CARES campaign, Atmos. Chem. Phys., 13,
721 2091-2113, 2013.

722 Singh, H. B., and Hanst, P. L.: Peroxyacetyl nitrate (PAN) in the unpolluted atmosphere: An
723 important reservoir for nitrogen oxides, Geophys. Res. Lett., 8, 941-944, 1981.

724 Sprengnether, M., Demerjian, K. L., Donahue, N. M., and Anderson, J. G.: Product analysis of
725 the OH oxidation of isoprene and 1, 3-butadiene in the presence of NO, J. Geophys. Res. Atmos.,
726 107, 10.1029/2001JD000716, 2002.

727 Surratt, J. D., Chan, A. W. H., Eddingsaas, N. C., Chan, M., Loza, C. L., Kwan, A. J., Hersey, S.
728 P., Flagan, R. C., Wennberg, P. O., and Seinfeld, J. H.: Reactive intermediates revealed in
729 secondary organic aerosol formation from isoprene, Proc. Natl. Acad. Sci. USA, 107, 6640-6645,
730 2010.

731 Teng, A. P., Crounse, J. D., and Wennberg, P. O.: Isoprene peroxy radical dynamics, J. Am.
732 Chem. Soc., 139, 5367-5377, 2017.

733 Thomas, D. A., Coggon, M. M., Lignell, H., Schilling, K. A., Zhang, X., Schwantes, R. H.,
734 Flagan, R. C., Seinfeld, J. H., and Beauchamp, J. L.: Real-time studies of iron oxalate-mediated
735 oxidation of glycolaldehyde as a model for photochemical aging of aqueous tropospheric
736 aerosols, Environ. Sci. Technol., 50, 12241-12249, 2016.

737 Tuazon, E. C., and Atkinson, R.: A product study of the gas-phase reaction of Isoprene with the
738 OH radical in the presence of NOx, Int. J. Chem. Kinet., 22, 1221-1236, 1990.

739 Wennberg, P. O., Bates, K. H., Crounse, J. D., Dodson, L. G., McVay, R. C., Mertens, L. A.,
740 Nguyen, T. B., Praske, E., Schwantes, R. H., Smarte, M. D., St Clair, J. M., Teng, A. P., Zhang,

741 X., and Seinfeld, J. H.: Gas-phase reactions of isoprene and its major oxidation products, Chem.
742 Rev., 10.1021/acs.chemrev.7b00439, 2018.

743 Xu, L., Guo, H., Boyd, C. M., Klein, M., Bougiatioti, A., Cerully, K. M., Hite, J. R., Isaacman-
744 VanWertz, G., Kreisberg, N. M., and Knote, C.: Effects of anthropogenic emissions on aerosol
745 formation from isoprene and monoterpenes in the southeastern United States, Proc. Natl. Acad.
746 Sci. USA, 112, 37-42, 2015.

747 Zhang, X., Chen, Z. M., and Zhao, Y.: Laboratory simulation for the aqueous OH-oxidation of
748 methyl vinyl ketone and methacrolein: significance to the in-cloud SOA production, Atmos.
749 Chem. Phys., 10, 9551-9561, 2010.

750 Zhang, X., and Seinfeld, J. H.: A functional group oxidation model (FGOM) for SOA formation
751 and aging, Atmos. Chem. Phys., 13, 5907-5926, 2013.

752 Zhang, X., Cappa, C. D., Jathar, S. H., McVay, R. C., Ensberg, J. J., Kleeman, M. J., and
753 Seinfeld, J. H.: Influence of vapor wall loss in laboratory chambers on yields of secondary
754 organic aerosol, Proc. Natl. Acad. Sci. USA, 111, 5802-5807, 2014a.

755 Zhang, X., Schwantes, R. H., Coggon, M. M., Loza, C. L., Schilling, K. A., Flagan, R. C., and
756 Seinfeld, J. H.: Role of ozone in SOA formation from alkane photooxidation, Atmos. Chem.
757 Phys., 14, 1733-1753, 2014b.

758 Zhang, X., McVay, R. C., Huang, D. D., Dalleska, N. F., Aumont, B., Flagan, R. C., and
759 Seinfeld, J. H.: Formation and evolution of molecular products in α-pinene secondary organic
760 aerosol, Proc. Natl. Acad. Sci. USA, 112, 14168-14173, 2015a.

761 Zhang, X., Schwantes, R. H., McVay, R. C., Lignell, H., Coggon, M. M., Flagan, R. C., and
762 Seinfeld, J. H.: Vapor wall deposition in Teflon chambers, Atmos. Chem. Phys., 15, 4197-4214,
763 2015b.

764 Zhang, X., Lambe, A. T., Upshur, M. A., Brooks, W. A., Gray Bé, A., Thomson, R. J., Geiger, F.
765 M., Surratt, J. D., Zhang, Z., and Gold, A.: Highly oxygenated multifunctional compounds in α-
766 pinene secondary organic aerosol, Environ. Sci. Technol., 51, 5932-5940, 2017.

767 Ziemann, P. J., and Atkinson, R.: Kinetics, products, and mechanisms of secondary organic
768 aerosol formation, Chem. Soc. Rev., 41, 6582-6605, 2012.
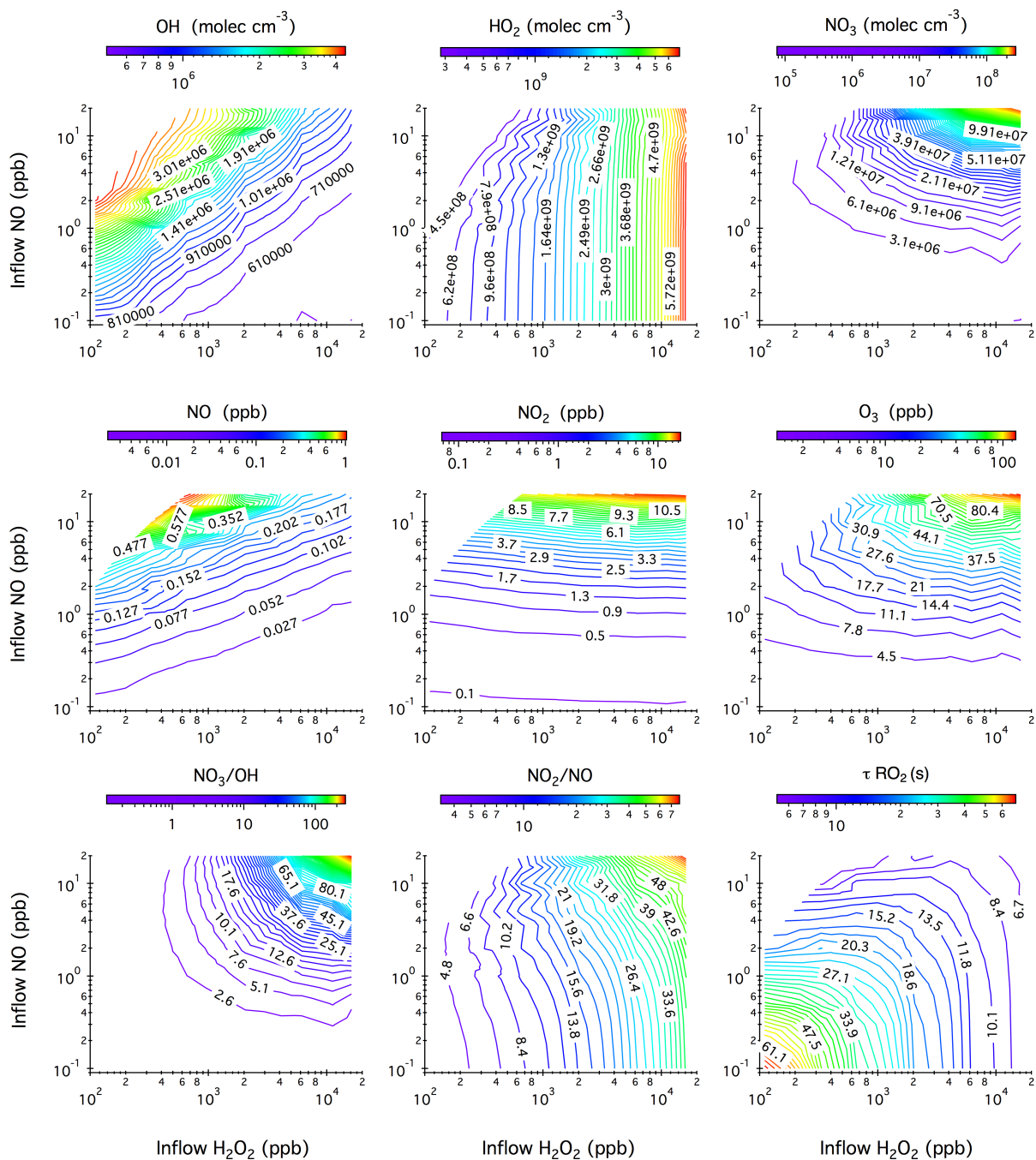
Figure 1. Contour plots showing the model predicted steady-state mixing ratios of OH, HO₂, NO₃, NO, NO₂, and O₃ after 20 hours of photochemical reactions in the chamber as a function of the concentrations of H_2O_2 and NO in the continuous injection flow. Also given here are the simulated NO₃ to OH ratio, NO₂ to NO ratio, and the lifetime of an RO₂ radical (τ_{RO_2}) with respect to reactions with NO and HO₂. Note that the ripples on the contour lines originate from the limited simulation datasets that are used to generate iso-response values.
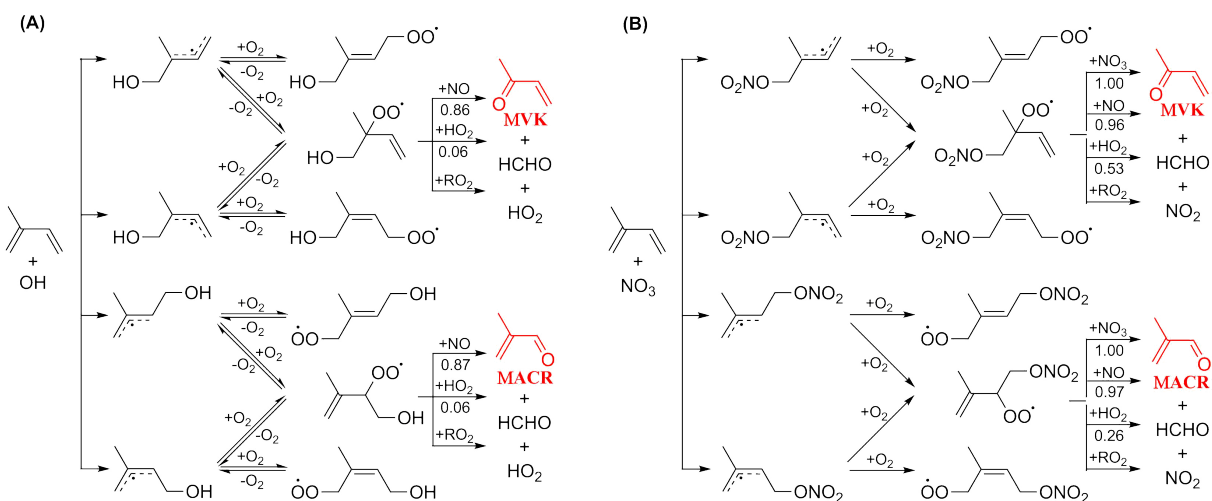
Figure 2. Representative mechanism for (A) OH- and (B) NO$_3$-initiated oxidation of isoprene that leads to the formation of MACR and MVK.
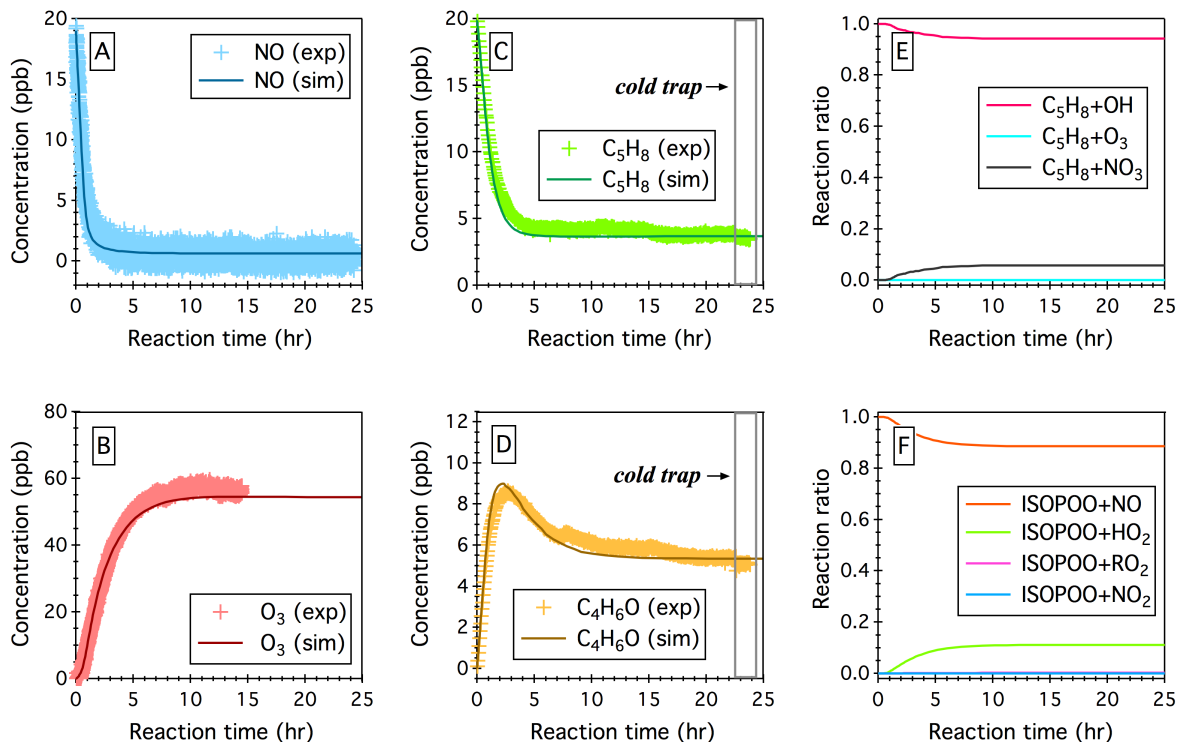
Figure 3. Simulated (sim.) and observed (exp.) temporal profiles of (A) NO, (B) O_3, (C) isoprene (C_5H_8), and (D) the sum of MACR and MVK (C_4H_6O) over 24 hours OH-initiated oxidation of isoprene in the continuous-flow mode chamber operation. Also displayed here include (E) simulated fractions of OH-oxidation, ozonolysis, and NO_3-oxidation as the removal pathways of isoprene, and (F) simulated fractions of ISOPOO radicals that react with NO, HO_2, RO_2, and NO_3. Time 0 is the point at which the chamber lights are turned on. Initial experimental conditions are 19 ppb NO, 0 ppb NO_2, 0 ppb O_3, 600 ppb H_2O_2, and 19.9 ppb C_5H_8, with continuous input of 600 ppb H_2O_2, 19 ppb NO, and 19.9 ppb C_5H_8 over the course of 24 hour photochemical reactions.
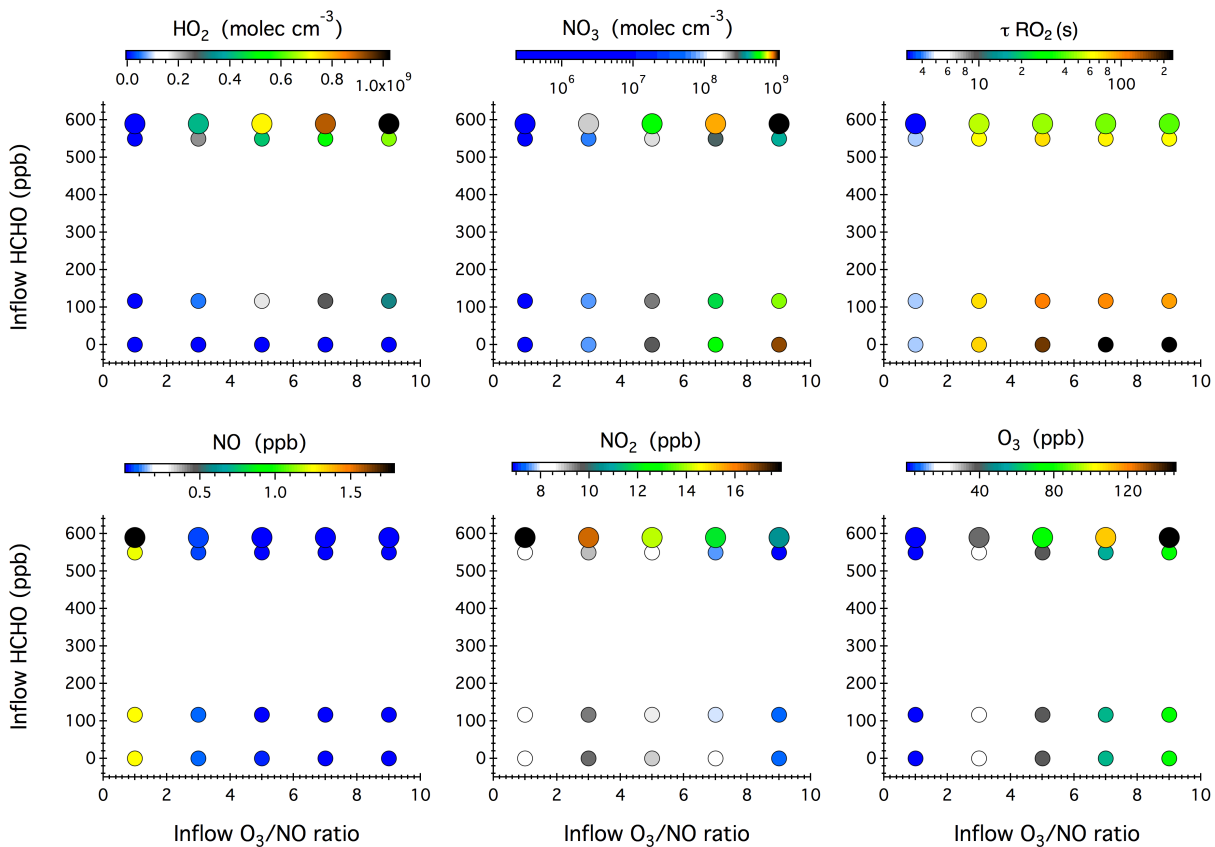
Figure 4. Simulated steady-state mixing ratios of HO_2, NO_3, NO, NO_2, and O_3 after 16 hours of dark reactions in the chamber as a function of the concentrations of NO and O_3 in the continuous injection flow. The symbol size denotes different inflow NO concentrations, i.e., 10 ppb and 20 ppb. Also given here is the calculated lifetime of an RO_2 radical (τ_{RO_2}) with respect to reactions with NO, NO_3, and HO_2.
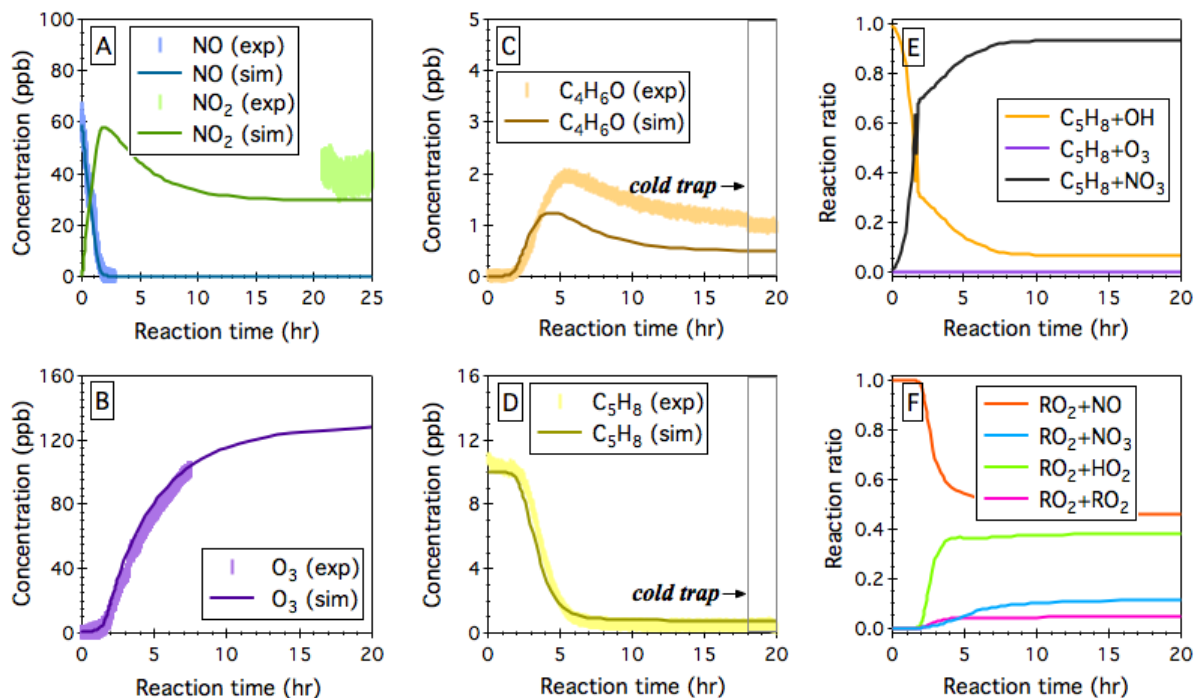
Figure 5. Simulated (sim.) and observed (exp.) evolution patterns of (A) NO_x, (B) O_3, (C) the sum of MACR and MVK (C_4H_6O), and (D) isoprene (C_5H_8) over 25 hours NO_3-initiated oxidation of isoprene under continuous-flow mode chamber operation. The fractions of isoprene that react with OH, O_3, and NO_3 are given in panel (E), and the fractions of INOO radical that undergo bimolecular reactions with NO, NO_3, HO_2, and RO_2 are given in panel (F). Initial experimental conditions are 0 ppb O_3, 59 ppb NO_x, and 10.2 ppb C_5H_8, with continuous input of 205 ppb O_3, 59 ppb NO, and 10.2 ppb C_5H_8 over the course of 25 hour dark reactions.